Journal of Photochemistry & Photobiology, B: Biology 210 (2020) 111961

Contents lists available at ScienceDirect

Journal of Photochemistry & Photobiology, B: Biology

journal homepage: www.elsevier.com/locate/jphotobiol

In vitro irradiation of doxorubicin with ^{18}F-FDG Cerenkov radiation and its potential application as a theragnostic system.

Hilda Angeline Quintos-Meneses[a,1], Liliana Aranda-Lara[a,1], Enrique Morales-Ávila[b,*], Eugenio Torres-García[c], Miguel Ángel Camacho-López[d], Mariana Sánchez-Holguín[e], Myrna A. Luna-Gutiérrez[f], Ninfa Ramírez-Durán[g], Keila Isaac-Olivé[a,*]

[a] Laboratorio de Investigación en Teranóstica. Facultad de Medicina, Universidad Autónoma del Estado de México, Toluca, 50180, Estado de México, Mexico.
[b] Laboratorio de Investigación Farmacia, Facultad de Química, Universidad Autónoma del Estado de México, Toluca, 50120, Estado de México, Mexico.
[c] Laboratorio de Dosimetría y Simulación Monte Carlo, Facultad de Medicina, Universidad Autónoma del Estado de México, Toluca, 50180, Estado de México, Mexico.
[d] Laboratorio de Fotomedicina, Biofotónica y Espectroscopía Láser de Pulsos Ultracortos. Facultad de Medicina, Universidad Autónoma del Estado de México, Toluca, 50180, Estado de México, Mexico.
[e] Departamento de Medicina Nuclear, Centro Oncológico Estatal-ISSEMyM, Toluca, 50180, Estado de México, Mexico
[f] Laboratorio Nacional de Investigación y Desarrollo de Radiofármacos-CONACyT, Instituto Nacional de Investigaciones Nucleares, Ocoyoacac, 52750, Estado de México, Mexico.
[g] Laboratorio de Microbiología Médica y Ambiental, Facultad de Medicina, Universidad Autónoma del Estado de México, Toluca, 50180, Estado de México, Mexico.

ARTICLE INFO

Keywords:
Doxorubicine·HCl
^{18}F-FDG
Cerenkov radiation
Photodynamic therapy
Chemotherapy-PDT system
Synergetic effect

ABSTRACT

Doxorubicin (DOX), an effective chemotherapeutic agent, has a wide excitation band centred at 480 nm. Cerenkov radiation (CR) is considered an internal light source in photodynamic therapy (PDT). DOX could be photoactivated by CR and thus, enhancing its cytotoxicity. In this work, ^{18}F-FDG was used to evaluate the effect of Cerenkov radiation on DOX, in comparison to irradiation with a 450-nm laser beam, in terms of ROS production. The production of $^1O_2$ and $O_2^{\cdot-}$ reactive species during DOX irradiation was detected indirectly by ABMA and DCPIP bleaching, respectively. The cytotoxic effect of the DOX / ^{18}F-FDG CR system was evaluated in the T47D breast cancer cell line. The irradiation of DOX produced $^1O_2$ and $O_2^{\cdot-}$ species using both ^{18}F-FDG CR and a 450-nm laser beam. The majority reactive species produced in both cases was $^1O_2$; a favourable result, given the greater cytotoxicity of this species. The viability of T47D cells in presence of DOX (5 nM), ^{18}F-FDG (37.5 μCi) and DOX (5 nM)/^{18}F-FDG (37.5 μCi) was (86 ± 9)%, (84 ± 8)% and (64 ± 5)%, respectively; these results suggest a synergistic cytotoxic effect derived from the cytotoxic activity of DOX and its photoactivation by ^{18}F-FDG CR. It is worth noting that the system could be optimized in terms of DOX concentration and ^{18}F-FDG activity for better results. Due to the fact that ^{18}F-FDG is widely used in nuclear imaging, the DOX/^{18}F-FDG system also possesses theragnostic characteristics. Thus, in this work, it is demonstrated that DOX can be used in a dual therapy system based on chemotherapy-PDT when ^{18}F-FDG CR is used as a DOX excitation source.

1. Introduction

Doxorubicin (DOX) is an anthracycline that has been used for more than 40 years as a chemotherapeutic agent in various types of haematological and solid cancers. The most-used chemical form in clinical practice is doxorubicin hydrochloride (DOX·HCl) [1]. The best-known side effect of DOX is cardiotoxicity, although myelosuppression, testicular and adipose tissue atrophy, liver damage, among others, have also been reported [1,2]. Such effects could be lessened by applying a lower dose of DOX, but the antitumour response would be compromised. A promising alternative is the use of adjuvant therapy, such as photodynamic therapy (PDT).

PDT is based on the formation of reactive oxygen species (ROS), when a photosensitizer (PS) accumulates in a pathological tissue and is excited with an appropriate wavelength, preferably in the presence of O_2 [3,4]. The resulting ROS cause irreversible damage to target cells. However, the photoactivation is limited to surface tissues when external light sources are used, reducing the treatment of deep tissues

* Corresponding authors.
E-mail addresses: emoralesav@uaemex.mx (E. Morales-Ávila), kisaaco@uaemex.mx (K. Isaac-Olivé).
[1] *Share first authorship*

https://doi.org/10.1016/j.jphotobiol.2020.111961
Received 8 April 2020; Received in revised form 18 June 2020; Accepted 12 July 2020
Available online 18 July 2020
1011-1344/

[4–6].

The emission and excitation spectra of DOX have allowed its application as a PS for PDT [7,8]. However, in order to use DOX as a PS in deep tissues, the excitation source must pass through the skin efficiently or be internalized at the target site. DOX has been used in chemotherapy-PDT combination therapies [4,9–11], but in these, DOX does not act as a PS.

In order to reach internal target sites, other photoactivation alternatives have been applied, such as: use of optic fibre probes [4], external irradiation based on non-linear effects [5], use of nano-flashing agents excited by X-ray sources to activate PS [6,12] and co-localization of the PS with a Cerenkov radiation-emitting radionuclide [12–16].

Cerenkov radiation (CR) occurs when a charged particle travels at a speed greater than the speed of light in a given dielectric medium, generating continuous emission of electromagnetic radiation in the UV–Vis region. This radiation has been used to generate optical images *in vivo* [17–19] and also as an alternative light source for PDT photoactivation [12–16]. Generally, beta-emitting radionuclides (β- or β +) are used as a CR source.

The intensity of the CR depends on the energy of the emitted particle, which should exceed an energy threshold value (~ 214 keV in water and 261 keV in tissue) [12]. CR intensity decreases as β particle energy decreases: ^{90}Y > ^{18}F > ^{131}I > ^{64}Cu > ^{177}Lu [20]. ^{18}F is convenient because it is a widely-used positron emitter for PET diagnosis and has been used as an internal source for PDT in preclinical studies [14,16]. When administered as ^{18}F-FDG, it accumulates naturally in proliferative tumour cells with negligible adverse effects on healthy tissues.

Since Cerenkov emission produces continuous radiation in the UV–Vis region and DOX has a wide excitation band centred at 480 nm, it is believed that CR excites DOX and produces ROS. This can be detected indirectly by ABMA and DCPIP. It is known that the toxicity of irradiated DOX is greater than its toxicity in the absence of light [7,10], so the DOX-CR combination would be a dual chemotherapy-PDT system that would allow lower doses of DOX to be administered and this would reduce side effects, without compromising its therapeutic action.

The objective of this work is to demonstrate the synergetic effect of chemotherapy-PDT when DOX is irradiated with CR from ^{18}F-FDG. The formation of reactive species $^1O_2$ and O_2^{*-}, using ABMA and DCPIP, respectively, as well as the cellular toxicity of the DOX/^{18}F-FDG system, are evaluated.

2. Materials and methods

2.1. General

2.1.1. Chemicals

Doxorubicin·HCl (DOX, Sigma Aldrich), 9,10-anthracenediyl-bis (methylene) dimalonic acid (ABMA, Sigma Aldrich), 2,6-dichlorophenolindophenol (DCPIP, Sigma Aldrich), ^{18}F-FDG, RPMI (Sigma Aldrich), foetal bovine serum (Gibco), penicillin-streptomycin (Gibco), XTT kit (Roche).

2.1.2. Irradiation at 450 nm

The irradiation of the solutions was carried out with a laser diode, at a power of 1400 mW. A 1-cm optical path quartz cuvette was located in the path of the light beam. To ensure irradiation of all the solution contained in the cuvette, the light beam was scattered with a diverging lens. All solutions were irradiated at the same position and distance from the diode. In all cases, the sample volume was 2 mL. DOX, ABMA and DCPIP solutions were irradiated alone and in mixtures at constant concentrations, recording the spectrophotometric changes during 35 min, at intervals of 5 min between irradiations. Fluor-18 was used in order to evaluate the effect of Cerenkov radiation on the photosensitizer. Chemical changes in the PS and radical production of the singlet oxygen (ABMA) and O_2^{*-} (DCPIP) were evaluated (Fig. 1).

2.1.3. UV–Vis determinations

All UV–Vis spectra were recorded in a double-beam PerkinElmer (Lambda 650) spectrophotometer using 1 nm resolution and 0.5 s of integration time, in the range 350–700 nm. In all cases 1-cm quartz cuvette was used. For guaranteeing minimal manipulation of spectra, same recording conditions were used in all cases.

2.1.4. Stock solutions

The following solutions were prepared with deionized distilled water (DDW): DOX·HCl (1 mg/mL), ABMA (100 μM) and DCPIP (932 μM).

2.2. Determination of the molar extinction coefficient of DOX

The molar extinction coefficient was calculated as the slope of the calibration curve constructed from the absorbance of standard solutions prepared from a 1000-ppm DOX stock solution. Standard solutions were prepared in DDW with the following concentrations: 50 ppm (8.6E-05 M), 33.30 ppm (5.7E-05 M), 25.00 ppm (4.3E-05 M), 16.70 ppm (2.9E-05 M), 12.50 ppm (2.2E-05 M), 8.35 ppm (1.4E-05 M), 6.25 ppm (1.1E-05 M) and 3.125 ppm (5.4E-06 M). The absorbance of each solution was measured from 380 to 680 nm. Three independent measurements were made for each concentration and the absorbances obtained were averaged at the maximum absorbance value (480 nm).

2.3. Irradiation of DOX, ABMA and DCPIP solutions with a 450-nm laser light

The 62.5-μg/mL DOX solution (125 μL of DOX (1 mg/mL) and 1875 μL of DDW), 50-μM ABMA solution (1000 μL of ABMA (100 μM) and 1000 μL of DDW) and 140-μM DCPIP solution (300 μL of DCPIP (932 μM) and 1700 μL of DDW) were individually irradiated for 35 min at 5-min intervals according to the geometry described in section 2.1.2. A DOX solution (62.5 μg/mL) without irradiation was used as a control. The UV–Vis spectrum was recorded. Each experiment was carried out in triplicate.

2.4. Irradiation of the DOX solution in the presence of ABMA with a 450-nm laser light

The solution prepared with 125 μL of DOX (1 mg/mL), 1000 μL of ABMA (100 μM) and 875 μL of DDW, with final concentrations of 62.5 μg/mL (DOX) and 50 μM (ABMA), was irradiated for 35 min at 5-min intervals according to the geometry described in section 2.1.2. After each irradiation, the UV–Vis spectrum was recorded. Each experiment was carried out in triplicate.

2.5. Irradiation of the DOX solution in the presence of DCPIP with a 450-nm laser light

The solution prepared with 125 μL of DOX (1 mg/mL), 300 μL of DCPIP (932 μM) and 1575 μL of DDW, with final concentrations of 62.5 μg/mL (DOX) and 140 μM (DCPIP), was irradiated for 35 min at 5-min intervals according to the geometry described in section 2.1.2. After each irradiation, the UV–Vis spectrum of the sample was recorded. Each experiment was carried out in triplicate.

2.6. Irradiation of DOX solution in the presence of ABMA and DCPIP with a 450-nm laser light

The solution prepared with 125 μL of DOX (1 mg/mL), 1000 μL of ABMA (100 μM), 300 μL of DCPIP (932 μM) and 575 μL of DDW, with final concentrations of 62.5 μg/mL (DOX), 50 μM (ABMA) and 140 μM (DCPIP), was irradiated for 35 min at 5-min intervals according to the described in 2.1.2 section. After each irradiation, the UV–Vis spectrum of the sample was recorded. Each experiment was carried out in

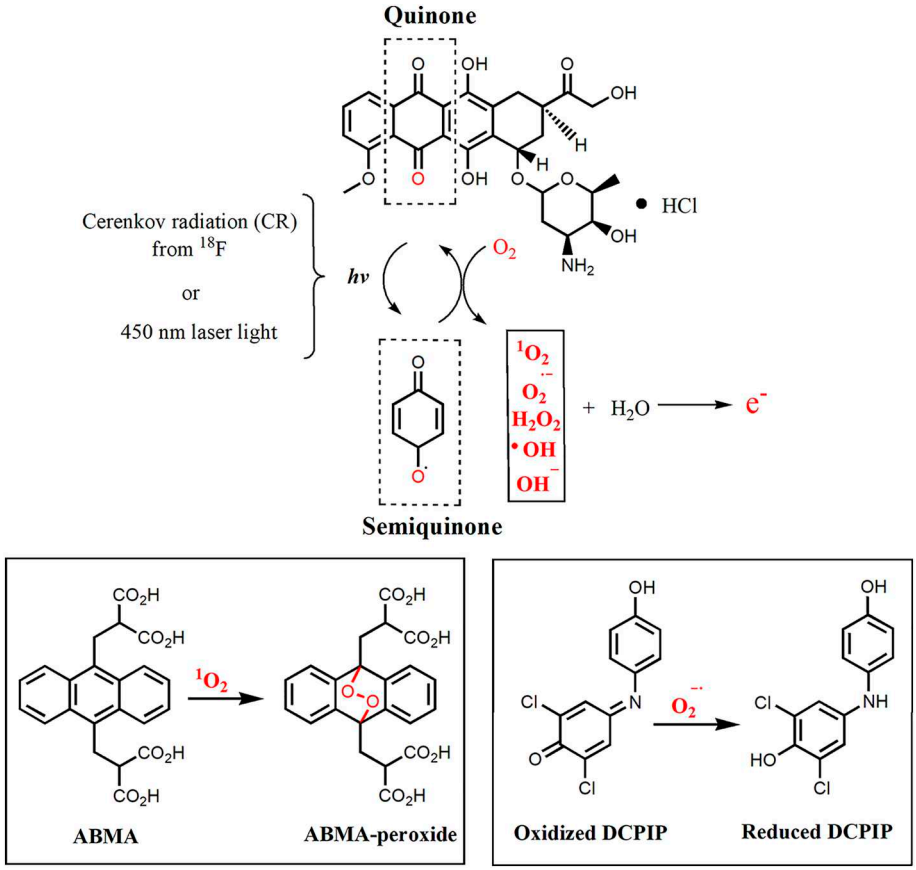

Fig. 1. Schematic description of the effect of a laser beam or Cerenkov radiation on the photosensitizer (DOX) and indicators of reactive oxygen species production.

triplicate.

2.7. Irradiation of the DOX solution in the presence of ABMA with Cerenkov radiation from ^{18}F-FDG

Six solutions were prepared with 125 μL of DOX (1 mg/mL) and 1000 μL of ABMA (100 μM). Volumes of 0 μL, 175 μL, 225 μL, 325 μL, 375 μL and 500 μL of ^{18}F-FDG (2 μCi/μL) were added to these solutions and the final volume was adjusted to 2 mL with DDW. The final samples had a concentration of 62.5 μg/mL (DOX), 50 μM (ABMA) and 0 μCi, 350 μCi, 450 μCi, 650 μCi, 750 μCi and 1000 μCi of ^{18}F-FDG, respectively. After 24 h of having added ^{18}F-FDG and kept the solutions in total darkness, UV–Vis spectra were recorded. Each experiment was carried out in triplicate.

2.8. Irradiation of the DOX solution in the presence of DCPIP with Cerenkov radiation from ^{18}F-FDG

Six solutions were prepared by mixing 125 μL of DOX (1 mg/mL) and 300 μL of DCPIP (932 μM). ^{18}F-FDG (2 μCi/μL) was added to the DOX/DCPIP mixture in the volumes of 0 μL, 225 μL, 325 μL, 375 μL, 450 μL and 500 μL; the final volume was adjusted to 2 mL with DDW. The final samples contained 62.5 μg/mL (DOX), 140 μM (DCPIP) and 0 μCi, 450 μCi, 650 μCi, 750 μCi, 900 μCi and 1000 μCi of ^{18}F-FDG, respectively. After 24 h of having added ^{18}F-FDG and kept the solutions in total darkness, UV–Vis spectra were recorded. Each experiment was carried out in triplicate.

2.9. In vitro studies

2.9.1. Cell culture

The T47D breast cancer cell line was originally obtained from ATCC (Atlanta, GA, USA). Cells were grown at 37 °C with 5% CO_2 and 85% humidity in RPMI medium supplemented with 10% foetal bovine serum and antibiotics (100 units/mL penicillin and 100 μg/mL streptomycin).

2.9.2. DOX dark toxicity

25,000 cells per well were seeded in a 96-well plate in 150 μL of fresh medium. The plate was incubated for 24 h at 37 °C with 5% CO_2 and 85% humidity in order for the cells to adhere. After the incubation period, 30 μL of the following DOX concentrations (nM) were added (n = 6): 0 (PBS 1×, pH 7.4, was added), 0.01, 0.05, 0.1, 0.5, 1, 5, 10, 100, 500, 1000 and 10000 nM. Once the treatments were added, the plate was returned to incubation and total darkness for another 24 h. After this time, cell viability was determined by means of the XTT assay. The IC_{50} was determined from a % cell viability *vs.* DOX concentration (nM) curve.

2.9.3. DOX/^{18}F-FDG cytotoxic effect

In 36 wells of a 96-well plate, 25,000 cells were seeded per well in 100 μL of RPMI medium supplemented with 10% foetal bovine serum and antibiotics (100 units/mL penicillin and 100 μg/mL streptomycin). One of the following treatments (n = 3 in all cases) were applied to the cells in suspension: (i) control, 100 μL of PBS 1×, pH 7.4; (ii) 50 μL of DOX (5 nM); (iii) 50 μL containing 17 μCi of ^{18}F-FDG; (iv) 50 μL containing 37.5 μCi of ^{18}F-FDG; (v) 50 μL containing 75 μCi of ^{18}F-FDG; (vi) 50 μL containing 112 μCi of ^{18}F-FDG; (vii) 50 μL containing 150 μCi of ^{18}F-FDG; (viii) 50 μL containing 17 μCi of ^{18}F-FDG and 50 μL of 5 nM DOX; (ix) 50 μL containing 37.5 μCi of ^{18}F-FDG and 50 μL of 5 nM DOX; (x) 50 μL containing 75 μCi of ^{18}F-FDG and 50 μL of 5 nM DOX; (xi) 50 μL containing 112 μCi of ^{18}F-FDG and 50 μL of 5 nM DOX; (xii) 50 μL containing 150 μCi of ^{18}F-FDG and 50 μL of 5 nM DOX. Once the treatments were applied, the cells were returned to incubation at 37 °C with 5% CO_2 and 85% humidity for 24 h. In those wells where the total

added volume was less than 100 μL, the required volume of PBS 1×, pH 7.4, was added in order to reach 100 μL. After the incubation period, cell viability was determined by means of the XTT assay.

2.10. Determination of the DOX/^{18}F-FDG combination index

From the IC_{50} values in T47D cells for DOX, ^{18}F-FDG and the 5-nM DOX/^{18}F-FDG combination, the combination index was determined by the equation:

$$CI = \frac{a}{A} + \frac{b}{B}$$

Where a is the IC_{50} value of the 5-nM DOX/^{18}F-FDG combination, b the value of the DOX in the DOX/^{18}F-FDG combination system (in this case, 5 nM), A is the IC_{50} due to ^{18}F-FDG and B is the IC_{50} of the DOX.

3. Results

3.1. DOX molar extinction coefficient

The linearity of the obtained calibration curve (molar concentration *vs.* absorbance) was satisfactory ($R^2 = 0.9919$). The highest % RSD value for the 3 independent absorbance determinations of the same concentration was 16%. The detection limit found was 9 ppm (1.6E-05 M). The slope of the calibration curve directly indicates the molar extinction coefficient. This was 10,067 M cm^{-1}, which is 95% in agreement with the 10,600 M cm^{-1} value mentioned by Parker et al. [21] and 97% with the 10,410 M cm^{-1} value mentioned by Yabbarov et al. [22].

3.2. Behaviour of DOX, ABMA and DCPIP solutions under 450-nm laser light irradiation

Fig. 2 shows the spectra obtained after the individual irradiation of DOX (Fig. 2a), ABMA (Fig. 2b) and DCPIP (Fig. 2c) with a 450-nm laser light for 35 min with 5-min intervals between irradiations. The analysis of absorbances at 450 nm shows significant alterations in the DOX spectra (Fig. 2d). The intensity of the maximum absorption decreases linearly as irradiation time increases, finding a 50% reduction of the initial absorbance, an expected phenomenon given its nature as a PS.

The ABMA and DCPIP spectra did not change their intensity and their maximum absorbance peaks did not shift during laser irradiation. The regions corresponding to the maximum absorbance peaks of ABMA (360 nm, 380 nm and 401 nm) and DCPIP (600 nm) in the DOX spectrum have low intensity. Thus, the UV–Vis quantification method has adequate specificity, since the analytes do not interfere with each other. These two aspects (no degradation and no interference) make such indicators useful to monitor ROS formation from DOX due to the excitation with a 450-nm laser light. It is important to note that, in the case of DOX irradiation, first-order kinetics were observed, with a negative rate coefficient related to DOX degradation (established using a $\ln [A] = \ln [A_0] - mt$ method and evaluated by linear least-squares analysis). A significant difference was found between DOX and ABMA or DCPIP spectra (Fig. 2d), where there were no apparent structural changes in ABMA and DCPIP after irradiation ($m \approx 0$).

The irradiation of DOX produced a shift in the absorption maximum towards the red. The maximum was found at 478 nm, between 0 and 5 min of irradiation and shifted to 481 nm after 10 and 15 min, and at 482 nm for the remainder of the experiment. To check whether the decrease in intensity and the shift of the absorption maximum were due to the action of light, the spectra of a non-irradiated DOX solution, prepared under the same conditions, was recorded. The non-irradiated solution showed no decrease or shift in the absorption (spectra not shown), demonstrating that both phenomena are dependent on irradiation with a 450-nm laser light.

3.3. Production of ROS during DOX irradiation with a 450-nm laser light

Fig. 3 shows the spectra obtained by irradiating the DOX with a 450-nm laser light in the presence of ABMA (Fig. 3a), and DCPIP (Fig. 3b). The irradiation of DOX/ABMA produced fading of the spectrum, proportional to the irradiation time. In this solution, the initial absorption maximum was 487 nm. This maximum was shifted to 484 nm after 5 min of irradiation and maintained that value until 15 min of irradiation. After the 20 min of irradiation, and until the end of the experiment, it was shifted to 483 nm; a value similar to that obtained at the end of the irradiation of DOX (alone) (482 nm). Significant photobleaching (and consequent loss of absorbance) was observed in wavelengths related to the ABMA absorption band. This is linearly related to photoinduced singlet oxygen generation from DOX to its corresponding endoperoxide.

The irradiation of the DOX/DCPIP solution produced a decrease in absorbance proportional to the irradiation time. In the DOX/DCPIP solution, the DOX maximum shifted to 502 nm and maintained that value throughout the irradiation period. The maximum absorbance values of the DCPIP were between 596 nm and 598 nm throughout the experiment. Due to the width of the band, such values were not considered as band shifting.

When the DOX solution was irradiated in presence of ABMA and DCPIP (Fig. 3c), a decrease in absorbance proportional to the irradiation time was observed. In this solution, the maximum of DOX was shifted to 509 nm and was kept at that value until 30 min of irradiation. It was then shifted to 511 nm to finish at a value of 517 nm after 35 min of irradiation. Of the ABMA peaks, the 401-nm peak remained stable at that position and the 360-nm and 380-nm peaks experienced a 1-nm shift. The DCPIP maintained its maximum between 590 and 597 nm, but due to the width of the band, it was considered a very slight shifting. The analysis of absorbance of the DOX band at 487 nm showed a kinetic behaviour with a rate coefficient similar to that obtained with the irradiated DOX solution (Fig. 3d).

3.4. Production of ROS during DOX irradiation with CR from ^{18}F-FDG

The DOX/ABMA solution, in the presence of different amounts of radiation from ^{18}F-FDG (Fig. 4a), produced a decrease in the absorbance of DOX/ABMA, proportional to the value of ^{18}F-FDG activity. The DOX/ABMA solution, previously irradiated with laser light, had the maximum absorption of DOX at $t = 0$ at 487 nm, representing a shift of 9 nm from DOX (alone). ^{18}F has the same effect as the laser beam; the DOX/ABMA solution had its absorption maximum at 487 nm. In the presence of 350 μCi of ^{18}F-FDG, the maximum was shifted to 492 nm; at 450 μCi and 650 μCi, it was kept at 494 nm; at 650 μCi, it was shifted to 496 nm and at 1000 μCi, the shift reached 502 nm.

With regard to the irradiation of the DOX/ABMA solution with the laser light, a hypsochromic shift was seen as the irradiation time increased. In this case, the opposite was observed, there was a bathochromic shift as the ^{18}F-FDG activity increased in the sample. Such shifts indicate changes in the molecule or its environment.

The DOX/DCPIP solution, in the presence of different amounts of ^{18}F-FDG (Fig. 4c), produced a decrease in the absorbance of DCPIP and DOX proportional to the value of the ^{18}F-FDG activity present. The DOX/DCPIP solution, previously irradiated with laser light, had the maximum absorption of DOX at $t = 0$ at 502 nm, representing a shift of 15 nm from DOX (alone). The DOX/DCPIP solution had its absorption maximum at 500 nm, whereas in the presence of 450 μCi of ^{18}F-FDG, the maximum was shifted to 501 nm, from 650 μCi at 502 nm, from 750 μCi at 503 nm, from 900 μCi at 505 nm and from 1000 μCi at 504 nm.

With regard to the irradiation of DOX/ DCPIP with the laser light, it was found that the maximum of DOX was maintained at 502 nm throughout the experiment. But in this case, a slight tendency to bathochromic shifts were observed as ^{18}F-FDG activity increased in the

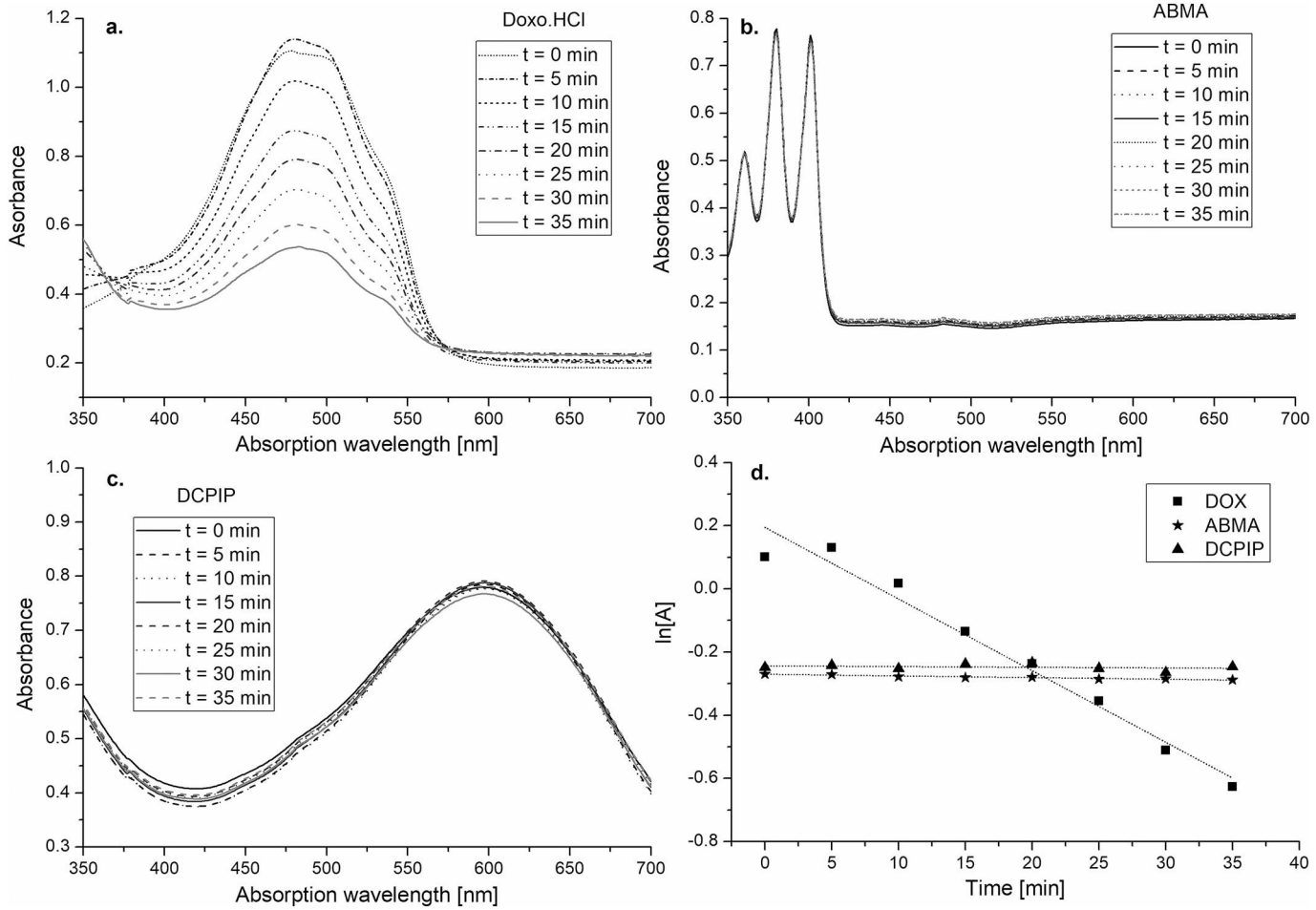

Fig. 2. Individual irradiation with a 450-nm laser diode of a. DOX, b. ABMA or c. DCPIP for 35 min, with 5-min intervals between irradiations and d. comparison of kinetic behaviour between DOX (487 nm), ABMA (401 nm) and DCPIP (596 nm).

sample.

The analysis of kinetic behaviour showed that, for both cases, ^{18}F-DOX/ABMA (Fig. 4b) and ^{18}F-DOX/DCPIP (Fig. 4d) had a negative rate coefficient related to DOX degradation and ABMA or DCPIP consumption, following a first-order reaction and linear dependency.

3.5. T47D cell proliferation studies

Fig. 5 shows the results obtained from *in vitro* studies with T47D cancer cells treated with DOX (dark toxicity) and DOX/^{18}F-FDG. The dark toxicity (Fig. 5a) shows that the IC_{50} value found for DOX (alone) was 0.58 μM. This value coincides (13% difference) with that reported for this type of cells by *www.cancerrxgene.org* (0.51 μM), although it deviates by 64% from that one (0.22 μM) reported by Iorio et al. [23]. In Fig. 5b, the first two bars (0 μCi) show cells untreated (left bar; 100% cell viability) and treated only with DOX (right bar; 86% cell viability). The addition of 17 μCi of ^{18}F-FDG did not lead to a significant difference in cell viability (98% cell viability with ^{18}F-FDG and 84% in DOX/^{18}F-FDG solution). With 37.5 μCi of ^{18}F-FDG, there was a significant decrease ($p < .01$ in all cases) of cell viability, both in the ^{18}F-FDG solution alone (37.5 μCi: 84%, 75 μCi: 49%, 112 μCi: 31% and 150 μCi: 21%), and the DOX/^{18}F-FDG combination (37.5 μCi: 64%, 75 μCi: 37%, 112 μCi: 20% and 150 μCi: 12%). A similar effect was found by Das et al. when simultaneously using DOX·azide-CR from ^{68}Ga [17]. The DOX·azide-^{68}Ga combination caused a significant decrease in cell viability compared to DOX·azide alone and ^{68}Ga alone. Similar results were also obtained using photosensitizing nanoparticles and ^{18}F-FDG as a source of CR [14].

To predict the type of effect produced, the combination index (CI) of the DOX/^{18}F-FDG combination was calculated. For this, the IC_{50} of the DOX (Fig. 5a), the IC_{50} of the ^{18}F-FDG (bars on the left, from Fig. 5b) and the IC_{50} of DOX/^{18}F-FDG (bars on the right, from Fig. 5b) were used. The result showed that the combination presents synergy, since the CI obtained was 0.75. This value can be optimized, since other DOX concentrations were not evaluated.

4. Discussion

The decrease in the absorbance of the DOX solution in the presence of a 450-nm laser light (Fig. 2a) is due to its nature as a PS. PS are modified to a one-electron reduction route, to produce the DOX-semiquinone radical by way of a non-enzymatic reaction, induced by the action of light in the presence of oxygen (photobleaching). By absorbing light of the appropriate wavelength, they pass from their ground state to a high-energy singlet state, which is rapidly lost by emission of light or heat. Alternatively, the singlet PS can go into a triplet state of lower energy, capable of participating in different chemical reactions that compete and give rise to various ROS, such as $^1O_2$ and $O_2^{\bullet-}$ [4,7,24]. The $^1O_2$ is formed when the PS in triplet state transfers its energy to the O_2 in ground state, which then passes to the singlet state ($^1O_2$). The $O_2^{\bullet-}$ is produced when the triplet state of the PS is reduced due to the transfer of an electron and, in reduced form, reacts with O_2 to produce $O_2^{\bullet-}$. If a proton is transferred instead of an electron, then other free radicals are produced that react in turn and, through a chain of reactions, can also produce $O_2^{\bullet-}$ [24]. All ROS present in solution contribute to chain reactions, thus producing PS photobleaching.

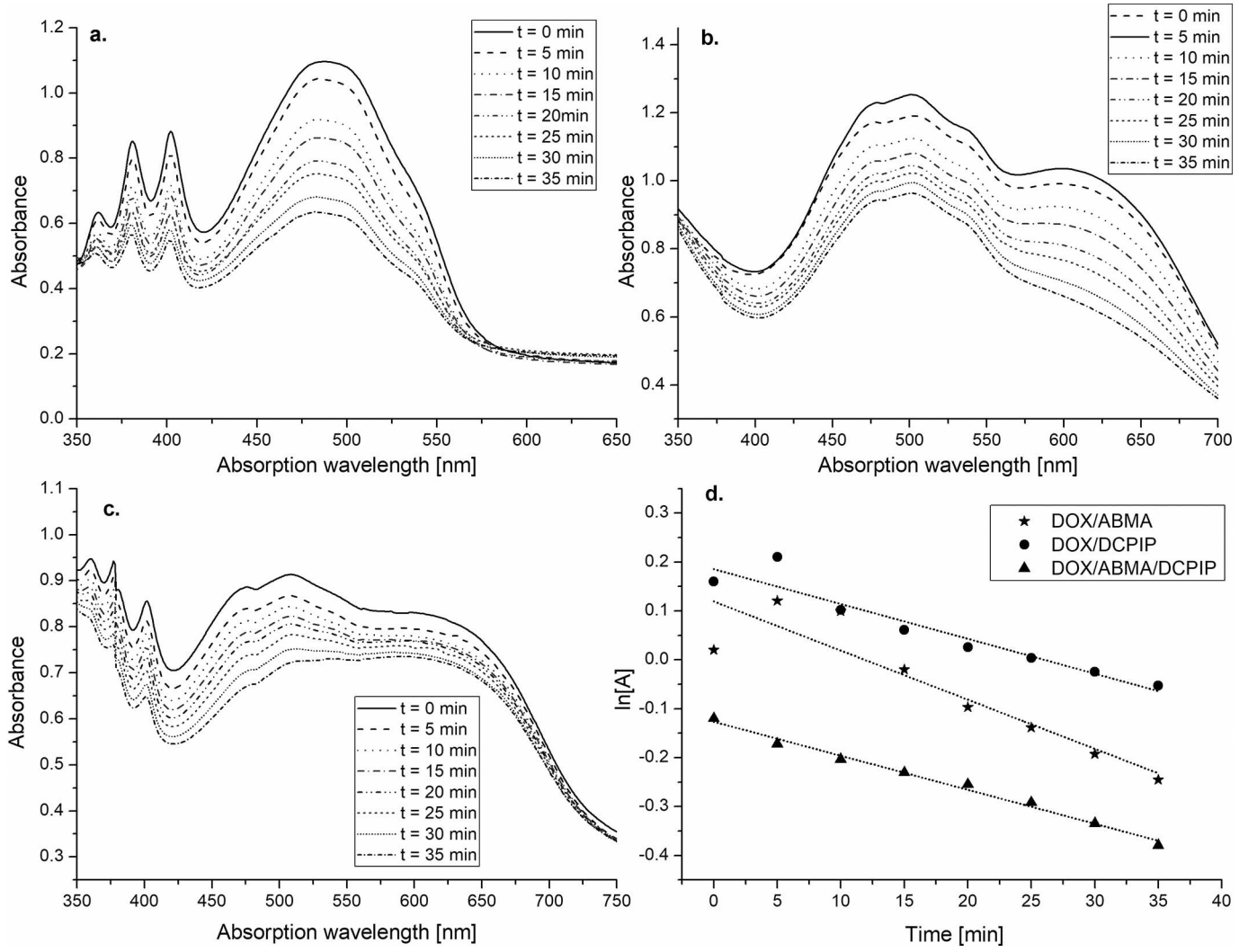

Fig. 3. Irradiation of DOX·HCl in the presence of ABMA (a), DCPIP (b), ABMA and DCPIP (c) at 450 nm for 35 min, with 5-min intervals between irradiations and (d) kinetic behaviour (487 nm).

A good PS must be able to produce ROS, in particular $^1O_2$, which is highly cytotoxic. The presence of $^1O_2$ and $O_2^{\bullet-}$ was determined qualitatively by irradiating DOX/ABMA and DOX/DCPIP solutions (Figs. 2b and 2c). Photobleaching of the DOX/ABMA solution indicates the presence of $^1O_2$ [25,26] and that of the DOX/DCPIP solution indicates the formation of $O_2^{\bullet-}$ [27].

From DOX, the values of maximum absorbance at different irradiation times were identified (Fig. 2a, 2b and 2c), DOX absorbance *vs.* irradiation time curves were constructed and fitted to straight lines. Absorbances at $t = 0$ were considered 100% of the DOX in the study solution. The slopes of these curves represent the DOX photobleaching rates in the different irradiated solutions, the values of which are shown in Table 1. Each point on the curve is the average of 3 independent repetitions. The maximum % RSD value of the curve points of the DOX, DOX/ABMA, DOX/DCPIP and DOX/ABMA/DCPIP solutions was 5%, 20%, 10% and 10%, respectively.

The results show that the DOX photobleaching rates decrease in the presence of ABMA and DCPIP, since these reagents act as scavengers of the ROS produced. When DOX is alone in solution, photobleaching is due to the generation of ROS, which are very reactive and "attack" it. In particular, $^1O_2$, due to its empty orbital, attacks the unsaturated bonds of DOX and produces its degradation by oxidation, with the consequent decrease in absorbance. In the presence of ABMA and DCPIP, the mechanism by which absorbance decreases is more complex, since the oxidation of DOX and the reactions of $^1O_2$ and $O_2^{\bullet-}$ compete with their respective monitor species. Consequently, the DOX photobleaching rates decrease due to the partial consumption of $^1O_2$ and $O_2^{\bullet-}$ caused by ABMA and DCPIP.

The photobleaching rates of the indicators in DOX/ABMA and DOX/DCPIP solutions, when solutions were irradiated with a 450-nm laser light, correlates positively with DOX degradation. The absorbances at $t = 0$ were considered 100% of ABMA and DCPIP in the respective maximum absorbance (401 nm and 596 nm, respectively) in the solution under study. The results obtained are shown in Table 2. As expected, photobleaching rates for DOX/ABMA and DOX/DCPIP solutions were higher than those for DOX/ABMA/DCPIP solution.

DOX concentration was the same in all solutions, but not ABMA and DCPIP concentrations. The concentrations were chosen in such a way that the absorbances of all its components were in the range of 0.8–1.0. If the photobleaching rate is normalized by the concentration of ABMA and DCPIP when each reagent is together with the DOX, the following is obtained: ABMA ($0.9387/50 = 0.0188\ min^{-1}\ \mu M^{-1}$), DCPIP ($1.2908/140 = 0.009\ min^{-1}\ \mu M^{-1}$) and an ABMA / DCPIP ratio = 2.1. Assuming that the reactions of ABMA and DCPIP with $^1O_2$ and $O_2^{\bullet-}$ respectively, are equimolar, the results indicate that the main species produced is $^1O_2$, since the photobleaching of the DOX/ABMA solution is greater than the DOX/DCPIP solution. This is clearly seen in Fig. 3, where the fading of the ABMA signal is greater than that of the DOX and

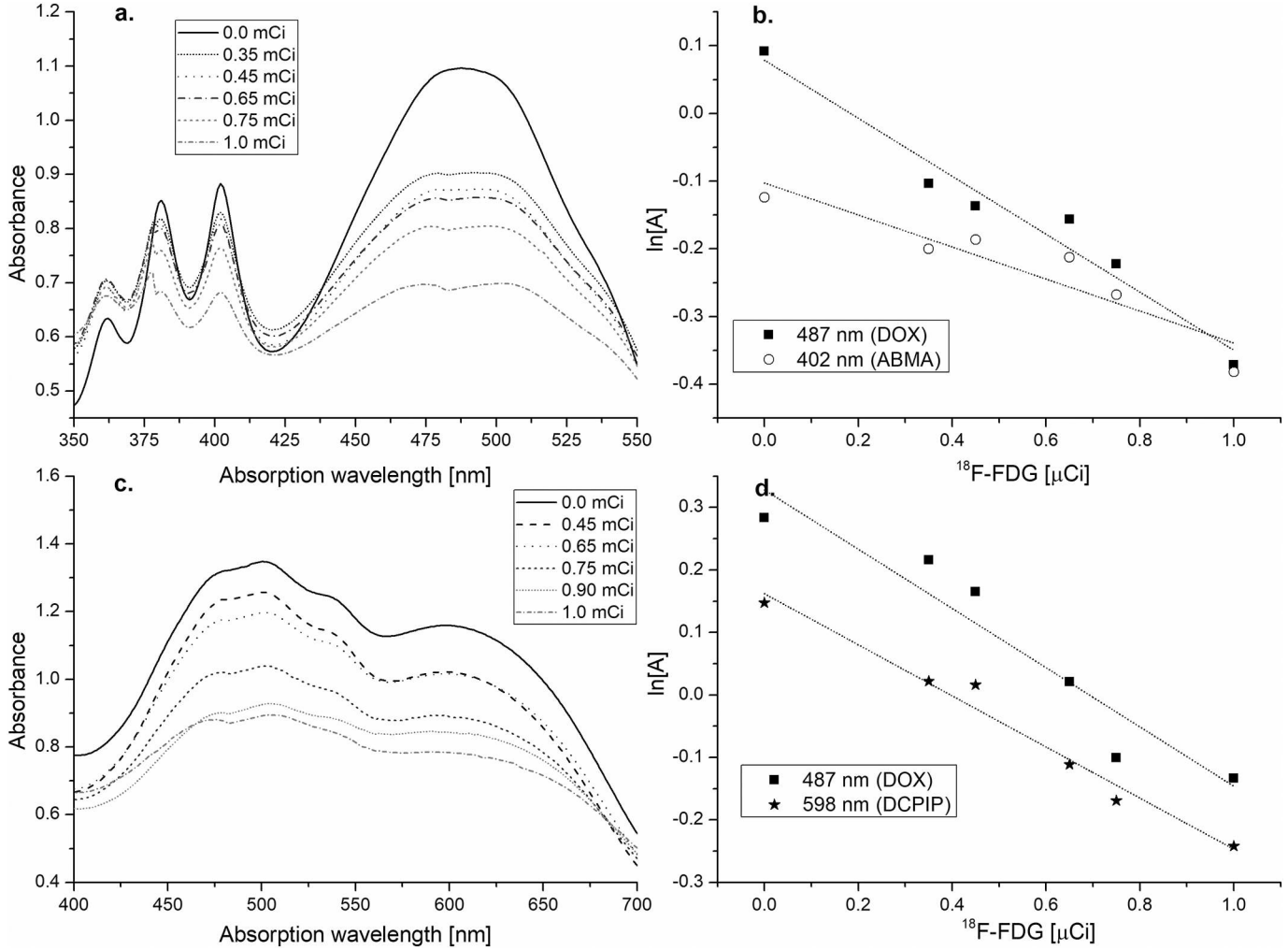

Fig. 4. (a) DOX in the presence of ABMA and different activities of ^{18}F-FDG; (b) kinetic behaviour of DOX and ABMA exposed to ^{18}F; (c) DOX in the presence of DCPIP and different activities of ^{18}F-FDG; (d) kinetic behaviour of DOX and DCPIP exposed to ^{18}F.

that of the DCPIP. These results confirm the effectiveness of doxorubicin as a photosensitizing agent.

DOX in the presence of various PS is known to enhance the effects of PDT [9–11,28] and its toxicity is significantly increased by irradiation with a 514- and 488-nm laser [7]. Such results indicate that DOX is a good candidate for a hybrid chemotherapy-PDT system, using DOX as a

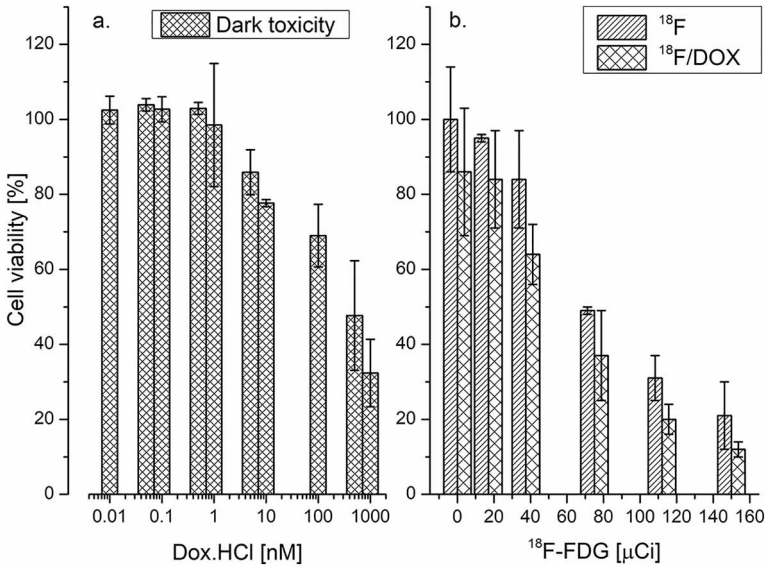

Fig. 5. (a) Cell viability of T47D cells treated with DOX (dark toxicity) and (b) effect on cell viability of ^{18}F and ^{18}F/DOX.

Table 1
Photobleaching rate of DOX irradiated with 450 nm in the presence of ABMA and/or DCPIP.

Solution	Rate (min^{-1})	Linearity (R^2)
DOX	1.6509	0.9731
DOX/ABMA	1.0693	0.9626
DOX/DCPIP	0.6765	0.8599
DOX/ABMA/DCPIP	0.5450	0.9863

Table 2
Photobleaching rates of ABMA and DCPIP in different solutions irradiated with a 450-nm laser light.

Solution	ABMA		DCPIP	
	Rate (min^{-1})	Linearity (R^2)	Rate (min^{-1})	Linearity (R^2)
DOX/ABMA	0.9387	0.9801	–	–
DOX/DCPIP	–	–	1.2908	0.9455
DOX/ABMA/DCPIP	0.6697	0.996	0.2885	0.9256

bifunctional agent.

Although DOX has low quantum yield [8,29], it would not impede its action as PS, because it also produces ROS through other redox mechanisms [2,7]. Motlagh et al. [8] reported a quantum yield value for DOX in DDW of 0.1, using Rhodamine 6G as a reference, while Shah et al. [29] reported a quantum yield value for DOX in PBS of 0.0444, using Rhodamine 101 as a reference.

In addition to the low quantum performance of DOX, probably another reason why PDT systems based exclusively on DOX have not been developed is due to the limited penetration of visible light (a few mm) into the tissue when it is externally irradiated. In order to irradiate DOX with visible light in PDT, optic fibres should be used, among other strategies, which make the treatment invasive, unless easily-accessible cavities such as cervix, are irradiated [4]. One option to overcome this disadvantage is to use an internal light source like CR.

With the Cerenkov effect, once the threshold energy is exceeded, the shape of the spectrum is the same regardless of the particle traveling in the medium. However, the intensity depends on the energy of the particle: the higher the energy, the higher the intensity. Liu reported that the intensity of the Cerenkov effect in β particle-emitting radionuclides (β + or β-) follows the following order: $^{90}Y > {}^{18}F > {}^{131}I > {}^{64}Cu > {}^{177}Lu$. In this work, the effect produced by the ^{18}F-FDG radiopharmaceutical, previously used for CR photoactivation, is reported [14,16,20,30].

Shah *et al* reported the DOX excitation spectrum, while Jimenez-Mancilla *et al* [29,31] proposed a mathematical model that reproduces the Cerenkov spectrum. For the 380 nm- 600 nm region, the mathematical function is:

$$I(\lambda) = A + \frac{B - C}{1 + 10^{(a-\lambda)(-b)}}$$

Where:
A = 0.1876, B = 1.0828, C = 0.1876,
a = 423.3840, b = 0.0216

Fig. 6 was made from the Cerenkov spectrum constructed by the mathematical model of Jimenez-Mancilla *et al* [31] and the excitation spectrum of DOX reported by Shah *et al* [29]. The figure shows that the wide excitation band of DOX overlaps with the spectrum of CR. It is an advantage to excite anthracycline with this light source. Thus, in theory, the CR of ^{18}F should excite DOX.

In practice, irradiation with ^{18}F-FDG of DOX/ABMA and DOX/DCPIP solutions produced photobleaching proportional to the activity of ^{18}F-FDG present (Fig. 4). DOX photobleaching in the presence of ABMA and DCPIP indicates formation of $^1O_2$ and $O_2^{\bullet-}$, due to the presence of a light source. The only light source in the experiment was the CR of the ^{18}F-FDG. Therefore, the CR of ^{18}F-FDG that affects DOX produces ROS in a similar way to the species that are produced when this compound is irradiated with a 450-nm laser light. Photoactivation with CR from ^{18}F-FDG has also been demonstrated by other authors [14,16,30].

There are different criteria regarding the usefulness of CR in PDT. Several authors [13,14,16] report positive results of PDT irradiated with CR. However, Klein *et al* [12] estimate that the effectiveness of PDT with CR is not due to the action of ROS that are generated by CR, but to a combination of alternative mechanisms such as direct excitation of PS and cellular radiosensitization due to ionizing radiation. Our work demonstrates that DOX produces ROS by irradiating with CR from ^{18}F-FDG, since the behaviour of DOX/ABMA and DOX/DCPIP solutions in the presence of ^{18}F-FDG was similar when irradiated with a 450-nm laser (Fig. 3).

The photobleaching rates of DOX/ABMA and DOX/DCPIP with CR from ^{18}F-FDG (Table 3) were determined analogously to the experiment with the 450-nm laser light (Tables 1 and 2). The results of Table 3 coincide with those obtained in Table 2. When irradiated with CR, the DOX/DCPIP solution had a higher photobleaching rate than the DOX/ABMA solution. Likewise, the relationship between the photobleaching rates normalized by the concentration of the indicators was similar (ABMA: 20.975/50 = 0.42 min^{-1} μM^{-1}; DCPIP: 31.6/140 = 0.22 min^{-1} μM^{-1} and ABMA/DCPIP ratio = 1.9), indicating that the majority species produced was $^1O_2$.

Finally, the *in vitro* study showed that with 37.5 μCi of ^{18}F-FDG, the viability of T47D cells in the presence of DOX/^{18}F-FDG decreases significantly ($p < .01$) in relation to those treated only with DOX. (Fig. 5a) or with ^{18}F-FDG (Fig. 5b; bars on the left). This dose-dependent decrease is attributed to the combined toxic effect of DOX, in its dual chemotherapeutic-PS function, and the interaction with cell tissue of both photons from positronic annihilation and CR from ^{18}F-FDG. The synergy of all these effects enhances the efficacy of the PDT-chemotherapy system. In *in vivo* experiments, a greater effect is to be expected, since CR increases with the transition from the refractive index of water (1.33) to that of biological tissue (> 1.40) [31].

Chemotherapy-PDT synergy is one of the many strategies that have been proposed to enhance the therapeutic outcome of low-dose chemotherapy and minimize its side effects [8,10,11,28]. However, in current PDT work with DOX, it is only used as a chemotherapeutic agent [9–11,28]. This work also exploits its possibilities as a PS, which will allow the design of a chemotherapy-PDT system with a more effective approach, which overcomes the difficulties of PDT with external radiation.

The cardiotoxicity of DOX, as well as toxicity to other organs and systems, is well-known and documented [1,2,11,32]. One of the strategies that have been proposed to decrease such effects is its encapsulation in different types of nanoparticles [9–11] that can specifically target the cancer cell. The vast possibilities offered by nanoparticles facilitate the future design of a system in which the residence time of the DOX-carrying nanoparticle is longer in the tumour cell than in the rest of the body. In this manner, after some time, the DOX will only be found in the target cell. At that moment, the administration of ^{18}F-FDG would safely allow the production of free radicals only in the malignant cell where this radiopharmaceutical usually accumulates [14,16]. The combination of DOX with PDT produced by CR would protect healthy tissue from the undesirable action of free radicals, since the path of CR in biological tissue is limited to 1–2 mm [12,16].

The low fluence rate of Cerenkov light emission from ^{18}F can be useful to guarantee a minimum oxygen depletion and less DOX degradation, since this drug forms ROS in the absence of radiation due to bioreduction [7,32]. A high fluence rate dramatically reduces the presence of O_2 in tumour tissue, which prevents the formation of new ROS and reduces the effectiveness of PS [4,13].

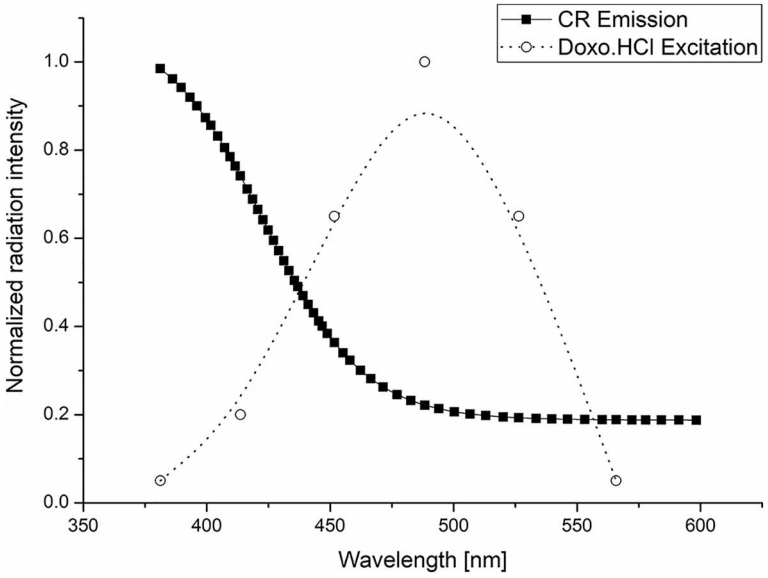

Fig. 6. Overlap of the normalized CR spectrum and the normalized DOX excitation band.

Table 3
Photobleaching rates of DOX / ABMA and DOX / DCPIP in different solutions irradiated with CR from ^{18}F-FDG.

	DOX		ABMA		DCPIP	
Solution	**Rate (min^{-1})**	**Linearity (R^2)**	**Rate (min^{-1})**	**Linearity (R^2)**	**Rate (min^{-1})**	**Linearity (R^2)**
DOX/ABMA	33.648	0.9546	20.975	0.8901	–	–
DOX/ DCPIP	35.373	0.8723	–	–	31.6	0.9264

A great advantage of using ^{18}F-FDG as a source of DOX excitation in a chemotherapy-PDT system is that ^{18}F can also be used to acquire positron emission tomography imaging. The dual functionality of a chemotherapy-PDT system allows it to have theragnostic applications.

5. Conclusions

This work demonstrates that CR from ^{18}F-FDG causes DOX photobleaching in a similar fashion to that when this anthracycline irradiated with a 450-nm laser. $^1O_2$ and O_2^{*-} are the main ROS that form during the 450-nm laser irradiation and CR exposure, which were confirmed by ABMA and DCPIP, respectively. $^1O_2$ is formed in a greater proportion than O_2^{*-}; a very favourable aspect, given the known cytotoxicity of this species. Cell viability experiments using T47D cells confirm the effectiveness of PDT, given the synergistic cytotoxic effect of the DOX/^{18}F-FDG combination. These results constitute the first step in the design of a PDT-chemotherapy theragnostic system using the CR of ^{18}F-FDG to photoactivate DOX. In such a system, DOX will act in its dual chemotherapeutic-PS character, the action of which can be monitored by means of the ^{18}F-FDG PET image, widely used for the detection of various types of tumours. Such a system would make it possible to significantly increase the effectiveness of PDT, particularly in deeply-located tumours, where external light does not reach, with the consequent decrease in undesirable effects from DOX. However, subsequent *in vivo* studies are required to verify the results obtained *in vitro,* preferably using DOX transport systems with specific recognition by tumour cells.

Conflicts of Interest

There are no conflicts to declare.

Declaration of Competing Interest

None.

Acknowledgements

This work was financially supported by the National Council for Science and Technology/Consejo Nacional de Ciencia y Tecnología (CONACyT) from Mexico, through the grant, with number SEP-CONACyT-CB-2016-01-287217. It was also carried out as part of the activities of the Laboratorio Nacional de Investigación y Desarrollo de Radiofármacos (LANIDER-CONACyT) (Mexico). The authors thank Dr. Eunice Olivé-Álvarez for her criticism, comments, and scientific discussions. The graduate student - scholarship granted to Hilda Angeline Quintos-Meneses from CONACyT through the Programa Nacional de Posgrados de Calidad (PNPC) is also acknowledged. She is graduate student from the Doctorate in Health Sciences at the Universidad Autónoma del Estado de México.

References

[1] S. Rivankar, An overview of doxorubicin formulations in cancer therapy, J. Cancer Res. Ther. 10 (2014) 853–858, https://doi.org/10.4103/0973-1482.139267.
[2] A. Pugazhendhi, T.N.J.I. Edison, B.K. Velmurugan, J.A. Jacob, I. Karuppusamy, Toxicity of doxorubicin (dox) to different experimental organ systems, Life Sci. 200 (2018) 26–30, https://doi.org/10.1016/j.lfs.2018.03.023.
[3] M. Tampa, M.-I. Sarbu, C. Matei, C.-I. Mitran, M.-I. Mitran, C. Caruntu, C. Constantin, M. Neagu, S.-R. Georgescu, Photodynamic therapy: a hot topic in dermato-oncology (review), Oncol. Lett. 17 (2019) 4085–4093, https://doi.org/10.3892/ol.2019.9939.
[4] A.F. Dos Santos, D.R.Q. De Almeida, L.F. Terra, M.S. Baptista, L. Labriola, Photodynamic therapy in cancer treatment - an update review, J. Cancer Metastasis Treat. 5 (2019) 25. doi:10.20517/2394-4722.2018.83.
[5] N. Malimonenko, A. Butenin, I. Mester, B. Kogan, Nonlinear photodynamic therapy using saturation of the photosensitizer triplet states, Laser Phys. Lett. 16 (2019)

055602, , https://doi.org/10.1088/1612-202X/ab0a5b.
[6] W. Sun, Z. Zhou, G. Pratx, X. Chen, H. Chen, Nanoscintillator-mediated X-ray induced photodynamic therapy for deep-seated tumors: from concept to biomedical applications, Theranostics. 10 (2020) 1296–1318, https://doi.org/10.7150/thno.41578.
[7] K.W. Lanks, J.-P. Gao, T. Sharma, Photodynamic enhancement of doxorubicin cytotoxicity, Cancer Chemother. Pharmacol. 35 (1994) 17–20, https://doi.org/10.1007/BF00686279.
[8] N.S.H. Motlagh, P. Parvin, F. Ghasemi, F. Atyabi, Fluorescence properties of several chemotherapy drugs: doxorubicin, paclitaxel and bleomycin, Biomed. Opt. Express. 7 (2016) 2400–2406, https://doi.org/10.1364/BOE.7.002400.
[9] Q. Tang, P. Hu, H. Peng, N. Zhang, Q. Zheng, Y. He, Near-infrared laser-triggered, self-Immolative smart Polymersomes for in vivo Cancer therapy, Int. J. Nanomedicine. Volume 15 (2020) 137–149, https://doi.org/10.2147/IJN.S224502.
[10] E.C. Aniogo, B.P.A. George, H. Abrahamse, In vitro combined effect of doxorubicin and sulfonated zinc Phthalocyanine–mediated photodynamic therapy on MCF-7 breast cancer cells, Tumor Biol. 39 (2017), https://doi.org/10.1177/1010428317727278.
[11] N.M. Candido, M.T. de Melo, L.P. Franchi, F.L. Primo, A.C. Tedesco, P. Rahal, M.F. Calmon, Combining photodynamic therapy and chemotherapy: improving breast Cancer treatment with nanotechnology, J. Biomed. Nanotechnol. 14 (2018) 994–1008, https://doi.org/10.1166/jbn.2018.2558.
[12] J.S. Klein, C. Sun, G. Pratx, Radioluminescence in biomedicine: physics, applications, and models, Phys. Med. Biol. 64 (2019) 04TR01. doi:https://doi.org/10.1088/1361-6560/aaf4de.
[13] B.A. Hartl, H. Hirschberg, L. Marcu, S.R. Cherry, Activating photodynamic therapy in vitro with Cerenkov radiation generated from Yttrium-90, J. Environ. Pathol. Toxicol. Oncol. 35 (2016) 185–192, https://doi.org/10.1615/JEnvironPatholToxicolOncol.2016016903.
[14] N. Kotagiri, G.P. Sudlow, W.J. Akers, S. Achilefu, Breaking the depth dependency of phototherapy with Cerenkov radiation and low-radiance-responsive nanophotosensitizers, Nat. Nanotechnol. 10 (2015) 370–379, https://doi.org/10.1038/nnano.2015.17.
[15] A. Kamkaew, L. Cheng, S. Goel, H.F. Valdovinos, T.E. Barnhart, Z. Liu, W. Cai, Cerenkov radiation induced photodynamic therapy using Chlorin e6-loaded hollow mesoporous silica nanoparticles, ACS Appl. Mater. Interfaces 8 (2016) 26630–26637, https://doi.org/10.1021/acsami.6b10255.
[16] Y. Nakamura, T. Nagaya, K. Sato, S. Okuyama, F. Ogata, K. Wong, S. Adler, P.L. Choyke, H. Kobayashi, Cerenkov radiation–induced Photoimmunotherapy with 18 F-FDG, J. Nucl. Med. 58 (2017) 1395–1400, https://doi.org/10.2967/jnumed.116.188789.
[17] S. Das, K. Haedicke, J. Grimm, Cerenkov-activated sticky tag for in vivo fluorescence imaging, J. Nucl. Med. 59 (2018) 58–65, https://doi.org/10.2967/jnumed.117.198549.
[18] A.E. Spinelli, M. Ferdeghini, C. Cavedon, E. Zivelonghi, R. Calandrino, A. Fenzi, A. Sbarbati, F. Boschi, First human Cerenkography, J. Biomed. Opt. 18 (2013) 020502, , https://doi.org/10.1117/1.JBO.18.2.020502.
[19] Y. Bernhard, B. Collin, R.A. Decréau, Redshifted Cherenkov radiation for in vivo imaging: coupling Cherenkov radiation energy transfer to multiple Förster resonance energy transfers, Sci. Rep. 7 (2017) 45063, https://doi.org/10.1038/srep45063.
[20] H. Liu, G. Ren, Z. Miao, X. Zhang, X. Tang, P. Han, S.S. Gambhir, Z. Cheng, Molecular optical imaging with radioactive probes, PLoS One 5 (2010) e9470, , https://doi.org/10.1371/journal.pone.0009470.
[21] M.A. Parker, V. King, K.P. Howard, Nuclear magnetic resonance study of doxorubicin binding to cardiolipin containing magnetically oriented phospholipid bilayers, Biochim. Biophys. Acta Biomembr. 1514 (2001) 206–216, https://doi.org/10.1016/S0005-2736(01)00371-6.
[22] N.G. Yabbarov, G.A. Posypanova, E.A. Vorontsov, O.N. Popova, E.S. Severin, Targeted delivery of doxorubicin: drug delivery system based on PAMAM dendrimers, Biochem. 78 (2013) 884–894, https://doi.org/10.1134/S000629791308004X.
[23] F. Iorio, T.A. Knijnenburg, D.J. Vis, G.R. Bignell, M.P. Menden, M. Schubert, N. Aben, E. Gonçalves, S. Barthorpe, H. Lightfoot, T. Cokelaer, P. Greninger, E. van Dyk, H. Chang, H. de Silva, H. Heyn, X. Deng, R.K. Egan, Q. Liu, T. Mironenko, X. Mitropoulos, L. Richardson, J. Wang, T. Zhang, S. Moran, S. Sayols, M. Soleimani, D. Tamborero, N. Lopez-Bigas, P. Ross-Macdonald, M. Esteller, N.S. Gray, D.A. Haber, M.R. Stratton, C.H. Benes, L.F.A. Wessels, J. Saez-Rodriguez, U. McDermott, M.J. Garnett, A Landscape of Pharmacogenomic Interactions in Cancer, Cell. 166 (2016) 740–754. doi:https://doi.org/10.1016/j.cell.2016.06.017.
[24] Q. Zheng, S. Jockusch, Z. Zhou, S.C. Blanchard, The contribution of reactive oxygen species to the Photobleaching of organic fluorophores, Photochem. Photobiol. 90 (2014) 448–454, https://doi.org/10.1111/php.12204.
[25] M.E. Alea-Reyes, M. Rodrigues, A. Serrà, M. Mora, M.L. Sagristá, A. González, S. Durán, M. Duch, J.A. Plaza, E. Vallés, D.A. Russell, L. Pérez-García, Nanostructured materials for photodynamic therapy: synthesis, characterization and in vitro activity, RSC Adv. 7 (2017) 16963–16976, https://doi.org/10.1039/C7RA01569K.
[26] J. Cáceres, J. Robinson-Duggon, A. Tapia, C. Paiva, M. Gómez, C. Bohne, D. Fuentealba, Photochemical behavior of biosupramolecular assemblies of photosensitizers, cucurbit[n]urils and albumins, Phys. Chem. Chem. Phys. 19 (2017) 2574–2582, https://doi.org/10.1039/C6CP07749H.
[27] C. Ikediobi, Bleaching of Dichlorophenolindophenol by a coupled oxidation with linoleate catalyzed by soybean lipoxygenase, Agric. Biol. Chem. 41 (1977) 2369–2375, https://doi.org/10.1080/00021369.1977.10862867.
[28] D. Dabkeviciene, A. Sasnauskiene, E. Leman, R. Kvietkauskaite, V. Kirveliene, Differential expression of VEGF and IL-1alpha after photodynamic treatment in combination with doxorubicin or taxotere, Anticancer Res. 34 (2014) 5295–5302 http://www.ncbi.nlm.nih.gov/pubmed/25275022.
[29] S. Shah, A. Chandra, A. Kaur, N. Sabnis, A. Lacko, Z. Gryczynski, R. Fudala, I. Gryczynski, Fluorescence properties of doxorubicin in PBS buffer and PVA films, J. Photochem. Photobiol. B Biol. 170 (2017) 65–69, https://doi.org/10.1016/j.jphotobiol.2017.03.024.
[30] C. Ran, Z. Zhang, J. Hooker, A. Moore, In vivo Photoactivation without “light”: use of Cherenkov radiation to overcome the penetration limit of light, Mol. Imaging Biol. 14 (2012) 156–162, https://doi.org/10.1007/s11307-011-0489-z.
[31] N.P. Jiménez-Mancilla, K. Isaac-Olivé, E. Torres-García, M.A. Camacho-López, G.J. Ramírez-Nava, H.J. Mendoza-Nava, Theoretical and experimental characterization of emission and transmission spectra of Cerenkov radiation generated by 177Lu in tissue, J. Biomed. Opt. 24 (2019) 076002, , https://doi.org/10.1117/1.JBO.24.7.076002.
[32] C.F. Thorn, C. Oshiro, S. Marsh, T. Hernandez-Boussard, H. McLeod, T.E. Klein, R.B. Altman, Doxorubicin pathways, Pharmacogenet. Genomics 21 (2011) 440–446, https://doi.org/10.1097/FPC.0b013e32833ffb56.